PAPER

Check for updates

Epidermal growth factor receptor targeted doxorubicin and vitexin loaded niosomes for enhanced breast cancer therapy†

S. Malathi,[a] Valappil Sisila,‡[b] V. Singaravel,‡[c] Nandakumar Venkatesan,[de] Iqbal Pakrudheen,[fg] R. Dhanaraj,[c] Niraikulam Ayyadurai,[b] V. Bhuvarahamurthy[c] and S. Narayana Kalkura [ID] *[a]

Breast cancer is one of the most frequently diagnosed cancers in women, and its current treatment modalities are limited by their non-specificity and adverse side effects. We evaluated the efficacy of cetuximab (C) conjugated doxorubicin (D) and vitexin (V) loaded niosomes (NIODVC) as a targeted delivery system for breast cancer. The combined release of doxorubicin and vitexin by antibody conjugated niosomes followed a biphasic release resulting in enhanced cytotoxicity (63%) and increased therapeutic efficiency compared to combined drug formulations (53%) without antibody. NIODVC demonstrated efficient cellular uptake *in vitro*, and its efficiency in treating breast cancer in BALB/c mice by local or systemic delivery was revealed by its potential anti-proliferation and anti-inflammatory activity. The localized delivery of NIODVC downregulated the genes that are over-expressed in breast cancer. These findings suggest that the combined delivery of doxorubicin and vitexin conjugated with cetuximab antibody provides a promising targeted therapy for breast cancer.

1. Introduction

Breast cancer is one of the most frequently diagnosed cancers in women globally with 2.26 million incident cases reported in 2020.[1] Triple-negative breast cancer has poor prognosis due to its ability to spread quickly and develop resistance to multiple drugs. The primary drugs used to treat advanced breast cancer conditions include doxorubicin and paclitaxel, which cause adverse effects as they target both cancerous and normal tissues, which could partly be attributed to the systemic delivery of these drugs.[2] In order to enhance the therapeutic efficiency of these drugs in targeting cancer cells and to reduce systemic toxicity, it is important to develop an alternative drug delivery system. Developing a targeted drug delivery system has significant advantages over conventional chemotherapy in breast cancer treatment, as it enables precise and effective delivery of therapeutic agents specifically to the tumor site.

The aim of the present study is to develop a targeted drug delivery system for breast cancer treatment. In this study, we aim to develop an endothelial growth factor receptor (EGFR) targeting niosome system to deliver doxorubicin and vitexin. Cetuximab was conjugated with the niosomes using gold nanoparticles as a linker. EGFR is highly expressed in most breast cancer which makes it an active target for delivery of drugs to breast cancer cells. Doxorubicin (D) is the most effective chemotherapeutic drug against triple-negative breast cancer (TNBC). The use of doxorubicin in treating TNBC is often limited due to several adverse reactions including fatigue, alopecia, nausea and vomiting, oral sores, bone marrow suppression and cardio toxicity. Doxorubicin induces oxidative stress, down regulates cardiac genes, apoptosis of cardiomyocyte and irreversible cardiomyopathy. The cardiotoxic mechanism is different from the anti-tumor mechanism of doxorubicin. This highlights the need to develop alternative ways to deliver doxorubicin and reducing its systemic toxicity.[3,4] Several studies have suggested that combining doxorubicin with flavonoids enhances the cytotoxic effect in tumor cells while protecting normal cells.[5–8]

[a] *Crystal Growth Centre, Anna University, Guindy, Chennai 600025, India.*
E-mail: kalkura@yahoo.com

[b] *Biochemistry & Biotechnology, CSIR-Central Leather Research Institute, Adyar, Chennai 600020, India*

[c] *Department of Medical Biochemistry, Post-graduate Institute of Basic Medical Sciences, University of Madras, Taramani, Chennai 600113, India*

[d] *Department of Pediatrics, Obstetrics, and Gynaecology, University of Valencia, Valencia, 46010, Spain*

[e] *Sri Ramachandra Faculty of Engineering and Technology, Sri Ramachandra Institute of Higher Education and Research, Chennai 600116, India*

[f] *Department of Chemistry, CMR Institute of Technology, Bengaluru 560037, India*

[g] *Centre of Excellence- Sensors & Nanoelectronics, CMR Institute of Technology, Bengaluru 560037, India*

† Electronic supplementary information (ESI) available. See DOI: https://doi.org/10.1039/d3ma00328k

‡ Equal contribution.

Vitexin (V), a flavone found in several medicinal plants, has numerous pharmacological effects, including anti-tumor, anti-oxidant, and anti-inflammatory effects.[9] It has been found that vitexin protects myocardial cells against the effects of hypoxia, specifically from reoxygenation injury,[10] and increases the bio-availability of drugs that are poorly soluble in water.

Niosomes (NIO) were selected in the present study as an alternative to the liposomal based drug delivery system.[11] Although liposomes have the capacity to incorporate both hydrophilic and lipophilic substances with low toxicity, the unique advantages of niosomes, including their ability to penetrate the stratum corneum and stability, make them a potential candidate for targeted drug delivery. Niosomes could encapsulate both hydrophilic and hydrophobic drugs within the aqueous core or between the membrane bilayers.[12,13] Niosomes are non-toxic,[14] non-ionic surfactant vesicles with good chemical stability at different storage temperatures and in different biological environments. They penetrate the stratum corneum by disrupting its structure and fluidic properties, resulting in an improved delivery of drugs.[15,16]

To achieve targeted delivery, niosomes were conjugated with cetuximab (C) monoclonal antibody. Cetuximab which is primarily an EGFR inhibitor is used to treat colorectal and head and neck cancer. It binds to the external domain of epidermal growth factor receptor (EGFR) and inhibits signal transduction by blocking ligand binding.[17–19] Gold nanoparticles were used to conjugate the antibody due to their excellent stability in solution, biocompatibility, and non-toxicity.[20–24] Electrostatic adsorption was used for antibody conjugation, utilizing the interaction between the positively charged amino acid residues on the antibody surface and the negatively charged gold nanoparticles.

2. Experimental

2.1. Materials

Span 80, cholesterol, cetuximab, doxorubicin, vitexin, gold(III) chloride trihydrate (HAuCl$_4$·3H$_2$O), dialysis membranes (MWCO 1000 Da) and trisodium citrate were purchased from Sigma Aldrich and used without further purification. Potassium carbonate, phosphate buffer saline (PBS), and phospho-tungstic acid were purchased from Sisco Research Laboratories Pvt. Ltd. Chloroform and methanol were purchased from Merck, India. The human triple-negative breast cancer cell line (MDA-MB-231) was purchased from the National Centre for Cell Science, Pune, India. Dulbecco's modified Eagle's medium (DMEM), fetal bovine serum (FBS), and 100× antimycotic solution were purchased from Sigma-Aldrich, USA. Dimethyl sulfoxide (DMSO) cell-culture grade, dimethyl thiazolyl tetrazolium bromide (MTT), fluorescein diacetate (FDA), and propidium iodide (PI) were purchased from HiMedia Laboratories, Mumbai, India.

2.2. Preparation of virgin and drug loaded niosomes

The thin film hydration method was used to prepare niosomes.[25] First, the non-ionic surfactant (Span 80) and cholesterol were dissolved in an equimolar ratio (0.1 M) in a
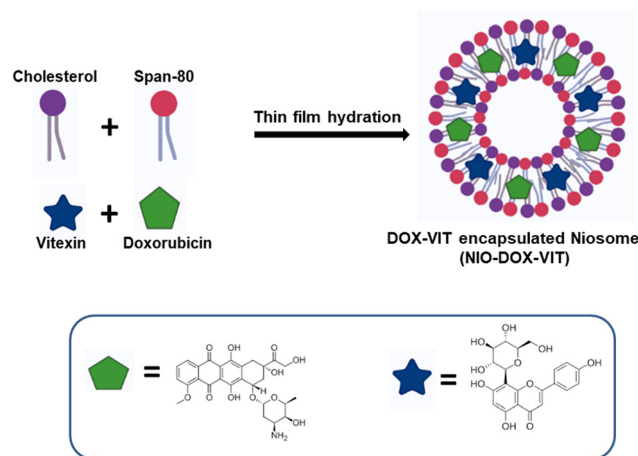
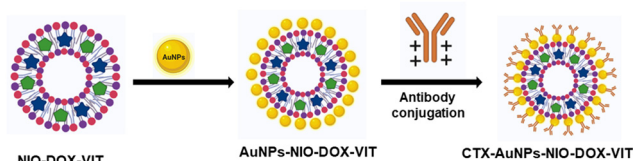**Scheme 1** Schematic representation of synthesis of drug loaded niosomes.

chloroform and methanol mixture (6 mL : 3 mL). The solvent was evaporated under vacuum using a rotary evaporator to form a thin film, which was further dried for 24 h in a vacuum desiccator. The film was then hydrated by resuspending in Milli-Q water (5 mL) and sonicated (M1800 ultrasonic bath) for 30 min to obtain niosomes. To prepare doxorubicin-loaded niosomes (NIOD), 100 μM doxorubicin was dissolved in 1 mL of PBS and added during the hydration step in the above mentioned procedure, followed by sonication to obtain doxorubicin-loaded niosomes. For vitexin-loaded niosomes (NIOV), 100 μM vitexin was dissolved in 1 mL of chloroform and added before the evaporation step. For doxorubicin- and vitexin-loaded niosomes (NIODV), the above procedures were carried out in the same suspensions (Scheme 1). Drug-loaded and virgin niosomes were stored at 4 °C until further use.

2.3. Synthesis of cetuximab conjugated niosomes

2.3.1. Synthesis of gold nanoparticles. Gold nanoparticles were synthesised by boiling 50 mL of 0.2 mM Au^{3+} (gold chloride trihydrate) and adding 1 mL of trisodium citrate (1%) under vigorous stirring.[26] The solution color changed from bluish-pink to ruby red after 10 min and the solution was continuously stirred at room temperature for 2 h. Nanoparticles were examined by ultraviolet-visible spectroscopy (UV-VIS) and transmission electron microscopy (TEM).

2.3.2. Synthesis of cetuximab conjugated niosomes. The first step in the synthesis of cetuximab-conjugated niosomes is to prepare gold nanoparticle bound niosomes (NION). Gold nanoparticles (10^{-4} M, 500 μL) were added to virgin and drug-encapsulated niosomes separately under continuous vigorous stirring for 30 min. The resulting mixture was centrifuged for 10 min, and the pellet was washed with deionized water three times to remove any unbound gold nanoparticles. The NION pellet was resuspended in deionized water, and the pH was adjusted to 8.0 using potassium carbonate (1%) to reach the isoelectric point of cetuximab. To facilitate antibody conjugation, a solution containing 100 μg of cetuximab in 50 μL was

Scheme 2 Schematic representation of conjugation of antibody to drug-loaded niosomes.

added to the mixture, and then stirred at 4 °C for 1 h.[27] The solution was then centrifuged at 15 000 rpm (4 °C) for 15 min, and the resulting pellet was washed with deionized water to eliminate any unconjugated antibodies. The same procedure was followed to prepare cetuximab-conjugated doxorubicin niosomes (NIODC), vitexin niosomes (NIOVC), and both doxorubicin and vitexin loaded niosomes (NIODVC), and the pellets were stored at −20 °C until further use (Scheme 2).

2.4. Characterization of niosome formulations

Cetuximab conjugated virgin and drug-loaded niosomes were characterized using a FTIR/ATR spectrometer (FTIR-JASCO-6300v, JASCO International Co. Ltd, Tokyo, Japan). The size and shape of gold nanoparticles were determined using a Talos F200S HRTEM (Thermo Fisher Scientific Inc, Waltham, MA, USA). The surface morphology was analyzed using a FEI Quanta FEG 200F HR-SEM. Dynamic light scattering (DLS) with a Zeta sizer Nanoseries (DLS-Malvern Zetasizer Nano-ZS) was used to measure the size and zeta potential. The encapsulation efficiency and the amount of drug released were quantified by UV-Visible spectroscopy (JASCO V-730 International Co. Ltd, Tokyo, Japan).[28]

2.5. Encapsulation efficiency of niosome formulations

To determine the encapsulation efficiency, the niosomes were solubilized in methanol. The amount of drug loaded was quantified using a UV-Visible spectrophotometer at 482 and 267 nm for doxorubicin and vitexin, respectively. All the experiments were performed in triplicate, and the encapsulation efficiency was determined by the following formula:

$$EE\% = (D_e/D_t) \times 100$$

where EE is the encapsulation efficiency, D_e is the amount of drug encapsulated and D_t is the total amount of drug.

2.6. In vitro drug release profile

The drug release kinetics of doxorubicin and vitexin from three different formulations NIOD, NIOV, and NIODV was determined by a dialysis method.[29] In brief, 100 mg of the sample was placed in a cellulose dialysis tubing membrane bag (MWCO: 1000 Da) and immersed in 100 mL of phosphate buffer saline (pH 7.4) at 37 °C under continuous stirring at 120 rpm. At different time intervals, 2 mL of released medium was collected. The amount of drug released was determined by measuring absorbance at 482 and 267 nm, and the cumulative

percentage of drug released from each niosome formulation was calculated.

2.7. Mathematical model of drug delivery

Different kinetic models were used to fit the drug release from different niosome formulations:

(1) Zero order release kinetics

$$C = C_0 + K_0 t$$

where C is the amount of drug released, K_0 is the zero-order constant, t is the time and C_0 is the initial amount of drug in solution.

(2) First order release kinetics

$$\log C = \frac{\log C_0 - K_1 t}{2.303}$$

where C_0 is the initial amount of drug, C is the percentage of drug released at time t and K_1 is the first-order constant.

(3) Higuchi kinetic model

$$Q = kH t^{1/2}$$

where Q is the percentage of cumulative amount of drug released at time t and kH is the Higuchi constant.

(4) Korsmeyer–Peppas kinetic model

$$\frac{C_t}{C_\infty} = K t^n$$

where C_t/C_∞ is the fraction of drug released at time t, K is the release rate constant and n is the release exponent.

(5) Hixson–Crowell model

$$Q_t^{1/3} = Q_0^{1/3} - kHC t$$

$$Q_0^{1/3} - Q_t^{1/3} = kHC t$$

where Q_0 is the initial weight of solid at time $t = 0$, Q_t is the remaining weight of solid at time t and kHC is the dissolution rate constant.

2.8. In vitro cytotoxicity of niosomes

2.8.1. Cell culture. MDA-MB-231, a human triple-negative breast cancer cell line, was cultured in Dulbecco's modified Eagle's medium supplemented with 10% fetal bovine serum at 37 °C. The cells were incubated in a humidified CO_2 incubator with 5% CO_2. Cells were trypsinized and cultured at a seeding density of 2×10^4 cells for 24 h before each experiment.

2.8.2. Cytotoxicity assay. The MTT assay was used to determine the cytotoxicity of all niosome formulations against the MDA-MB-231 cell line. The niosomes were filter sterilized using a 0.22 μm syringe filter and UV sterilized (1 h in laminar hood). 3×10^3 cells per well were seeded in a 96-well plate and incubated for 24 h. Cells were then treated with different concentrations (0–50 μg mL⁻¹) of niosomes and incubated for 24 h. Virgin niosomes without drugs were used as controls. The experiments involved the use of controls, including PBS (negative control), niosome (vehicle control), and Doxorubicin

(positive control). After 24 h, 100 μL of 3-(4,5-dimethylthiazol-2-yl)-2,5-diphenyltetrazolium bromide solution (2 mg mL^{-1}) was added to each well and incubated for 4 h. The culture medium was then removed carefully, and the formazan crystals formed were resuspended in 100 μL of DMSO. The absorbance was measured at 570 nm using the Epoch 2 microplate reader, and the percentage of viable cells was calculated:

$$\text{Cell viability (\%)} = \frac{\text{Absorbance of samples} \times 100}{\text{Absorbance of control}}$$

2.8.3. Live/dead cell assay. Live/dead cell assay was performed to visualize the morphological changes associated with the treatment of niosome formulations. MDA-MB-231 cells were seeded at a density of 3×10^3 cells per well in a 96 well plate and cultured for 24 h. Cells were treated with all niosome formulations individually at a concentration of 1 μg mL^{-1} and incubated for another 24 h. Later the medium was removed and the cells were washed with PBS ($1\times$) for 5 min. Cells were then incubated with fluorescein diacetate (400 nM) and propidium iodide (1 μM) for 2 min. Stained cells were visualized under a fluorescence microscope (DMi8, Leica Microscopy, Germany).

2.8.4. Cellular uptake of drug loaded niosomes. MDA-MB-231 cells were seeded at a density of 3×10^3 cells per well in a 48 well plate and cultured for 24 h. Later, the cells were treated individually with all niosome formulations at a concentration of 1 μg mL^{-1} for 24 h. The cells were washed twice with PBS, trypsinized and resuspended in 400 μL of PBS, and the cellular uptake of niosomes was determined by the fluorescence intensity of doxorubicin using a fluorescence microscope.

2.9. *In vivo* efficiency of cetuximab conjugated drug loaded niosomes

Female BALB/c mice aged 8 to 10 weeks were used. The animal use and all procedures were approved by the Institutional Animal Ethics Committee (IAEC) (205/GO/ReBi-S/Re-1/2000/CPCSEA) of the Central Animal House Facility, Dr ALM PG-IBMS, University of Madras, Taramani Campus, Tamilnadu, India. A total of 30 mice were used in the present study; the animals were provided with unrestricted access to food and monitored regularly in a pathogen-free and controlled environment. Breast cancer was induced in BALB/c mice using 4T1 breast cancer cells.[30] Mice were anaesthetized under general anaesthesia (ketamine at 100 mg kg^{-1} body weight). The body was shaved from the fourth nipple to the midline, and 4T1 cells at a density of 5×10^5 cells were suspended in an equal volume of serum free media and matrigel (100 μL) and injected into the fourth inguinal mammary fat pad. The tumor development was monitored by measuring tumor volume regularly using the following formula:[31]

$$T_v = D_s{}^2 \times D_l \times \pi/6$$

where T_v is the tumor volume, D_s is the shortest diameter of the tumor and D_l is the longest diameter of the tumor.

When the tumor volume reached a minimum volume (150 mm^3), the animals were divided into six different groups randomly with each group consisting of 5 animals. Of the six different groups two groups were randomly selected for localized delivery and another two for systemic delivery. Group I: control, group II: tumor control, group III: NIODV (local), group IV: NIODV (intravenous), group V: NIODVC (local), and group VI: NIODVC (intravenous). A single dose of niosome formulation contained doxorubicin (4 mg kg^{-1}), vitexin (20 mg kg^{-1}), and cetuximab (4 mg kg^{-1}). For localized delivery, niosomes were injected at the fourth inguinal mammary fat pad, and for systemic delivery, the niosomes were injected intravenously through the caudal vein. During the study, the animals were weighed regularly and the tumor dimensions were measured daily and recorded up to 20 days (Fig. 1). The mice were euthanized on day 20, and the tumor was excised and weighed. The vital organs (liver, spleen, kidney, heart, and lungs) were removed from each animal, washed with phosphate buffered saline, and weighed individually and proceeded for histology and gene expression studies.

2.9.1. Quantitative real-time PCR assay. RNA was extracted from the mammary tissues using Trizol by a method reported earlier.[32] The quality and quantity of RNA were analysed using a NanoDrop-spectrophotometer (Thermo 2000/2000c). RNA was reverse transcribed into cDNA using an Invitrogen SuperScript III First Strand synthesis kit following the manufacturer's protocol. The expression profile of selected genes, including BRCA1, EpCAM, C-MYC, NFKB, MMP9, miCAM, and iNOS, was determined by qPCR (CFX96 Touch Real-Time PCR Detection System, Bio-Rad) using SYBR green chemistry from Biorad (SsoAdvanced – Universal SYBR Green supermix). The amplification conditions employed were as follows: an initial denaturation step at 95 °C for 10 minutes, followed by 40 cycles of denaturation at 95 °C and annealing/extension at 55–60 °C for 15–30 seconds.[33] β-Actin was used as the housekeeping gene. The primer sequence of all the genes tested is tabulated in Table 1.

2.9.2. Histological analysis. Paraformaldehyde (4%) fixed mammary tissues were rehydrated and subsequently dehydrated using graded series of ethanol and embedded in paraffin wax. Sections of 4 μm thick were cut using a rotary microtome (Leica Rm2245) and the sections were stained with haematoxylin and eosin by the conventional method and visualized under a light microscope.[34] Immunohistochemistry of Ki67 (Abcam ab15580) and PCNA (BioGenex AM252-5M) was carried out on de-paraffinized tissue sections following the guidelines provided by the respective manufacturers.

2.10. Statistical analysis

The results were presented as the mean value plus or minus standard error. Statistical analysis was carried out using Graph Pad Prism (version 9), and a *P* value <0.05 was considered as statistically significant.

3. Results and discussion

3.1. Characterization of niosome formulations

We examined the physicochemical properties of the niosomes, including size, morphology, surface charge, and their cytotoxicity

Fig. 1 Representative photographs of tumor induced mice before and after treatment.

Table 1 List of genes and primer sequences used in the real-time qPCR analysis

Gene name	Sequence of primers (5′-3′)
BRCA1	FP: CCACAGTGGGCTTACCTGTT
	RP: GAGTCCATTCTCCCCGCTTC
C-MYC	FP: CCTGCTTCTGGAGGGTGATG
	RP: TGATGTGGTGTCTTGGAGAA
EpCAM	FP: CATTTGCTCCAAACTGGCGT
	RP: TTGTTCTGGATCGCCCCTTC
iNOS	FP: GCACCGAGATTGGAGTTC
	RP: GAGCACAGCCACATTGAT
miCAM	FP: TGCTCAGGTATCCATCCATCC
	RP: ACGGTGCCACAGTTCTCAA
MMP9	FP: GCCGACTTTTGTGGTCTTCC
	RP: GGTACAAGTATGCCTCTGCCA
NFKB	FP: CCTGCTTCTGGAGGGTGATG
	RP: GCCGCTATATGCAGAGGTGT
β-Actin	FP: TTCCAGCCTTCCTTCTTG
	RP: GAGCCAGAGCAGTAATC

against the triple-negative breast cancer MDMB-231 cell line. The average diameter of all the niosome formulations, polydispersity index (PDI), encapsulation efficiency (EE%), zeta potential, and the cumulative drug released at the end of 96 h are tabulated (Table 2). The average diameter of virgin niosomes was 380 ± 1.00 nm, but loading with doxorubicin, vitexin, and both doxorubicin and vitexin resulted in an increase in size to 410 nm ± 1.20, 389 nm ± 2.10, and 420 nm ± 1.00, respectively. The increase in size could be attributed to the rigidity of the bilayer

in the liquid phase due to the addition of drugs.[35] NIOD had a larger particle size than NIOV which is due to the higher molecular weight of doxorubicin. The average size of citrate stabilized gold nanoparticles was 30 nm. However, after the conjugation of the niosomes with cetuximab and gold nanoparticles, there was a significant increase in the size of the niosomes (425 nm ± 1.15). It has been reported that particles of size 425 nm are suitable for accumulation in solid tumor through the enhanced permeability and retention (EPR) effect or the passive targeting mechanism.[36] For colloidal systems used in drug delivery, a polydispersity index (PDI) of less than 0.3 indicates a homogeneous population. The PDI values for all the niosome formulations ranged from 0.199 to 0.321, suggesting that the niosomes were relatively uniform in size.[37] Zeta potential was measured to determine the stability of the formulations; values close to ±30 mV indicate a stable formulation.[38] Zeta potential values of NIO, NIOD, NIOV, and NIODV were −28 ± 0.45, −29 ± 0.25, −34 ± 0.58, and −37 ± 0.56 mV, indicating that the niosome formulations without the antibody conjugation were having a negative charge.[39] In the case of cetuximab-conjugated niosomes, citrate was used as a reducing agent in the synthesis of gold nanoparticles, which induced a negative charge on the surface of the nanoparticles, resulting in a Zeta potential of −22 ± 0.44 mV which prevents the nanoparticles from aggregation and precipitation over time (Table 2).[40] Krasnici et al. found that cationic liposomes preferentially target the angiogenic endothelium of tumors.[41] Similarly, Li et al. reported enhanced pulmonary insulin absorption compared to neutral liposomes.[42] The encapsulation efficiencies for doxorubicin and vitexin were 72% and 81%, respectively. When both drugs were loaded together (NIODV), the encapsulation efficiencies for doxorubicin and vitexin were found to be 73% and 83%, respectively. Higher encapsulation efficiency for vitexin could be attributed to its lipophilicity; similar results were observed with apigenin liposomal formulations by Banerjee et al.[43]

The FTIR spectrum of virgin niosomes (Fig. 2A) showed a characteristic ester peak at 1736 cm^{-1} that corresponds to Span 80 and a cholesterol hydroxyl peak at 3411 cm^{-1}. The peak at

Table 2 Physicochemical properties of niosome formulations

Sample	Average vesicle diameter (nm)	PDI	Zeta potential (mV)	Encapsulation efficiency (%)	Cumulative drug release (%)
NIO	380 ± 1.00	0.321 ± 0.03	-28 ± 0.45	0	—
NIOD	410 ± 1.20	0.28 ± 0.05	-29 ± 0.25	72.75 ± 0.96	71%
NIOV	389 ± 2.10	0.199 ± 0.03	-34 ± 0.58	81.12 ± 0.12	53%
NIODV	420 ± 1.00	0.201 ± 0.04	-37 ± 0.56	DOX:73.98 ± 0.56	85%
				VIT:83.98 ± 0.75	67%
Gold nanoparticles (N)	030 ± 0.005	—	-22 ± 0.44	—	—
NIODVN	424 ± 1.25	0.271 ± 0.01	-34 ± 0.86	—	—
NIODVC	425 ± 1.15	0.291 ± 0.04	-35 ± 0.46	—	—
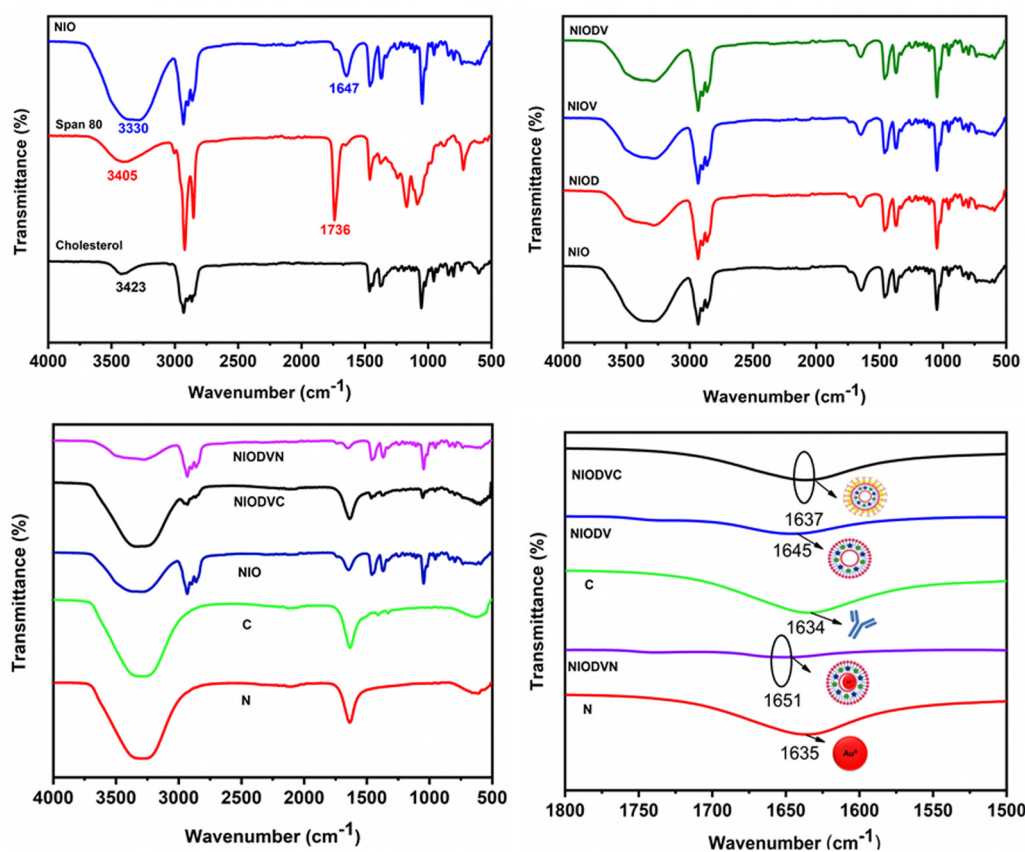
Fig. 2 FTIR spectra of blank niosomes (A), drug loaded niosomes (B), and gold nanoparticle and antibody-conjugated drug loaded niosome vesicles (C), and magnified view of the spectral region between 1800 and 1500 cm^{-1} (D).

1647 cm^{-1} confirmed the presence of hydrogen bonding between the carbonyl and the hydroxyl group of span 80 and cholesterol.[44] The structural integrity of the niosome is maintained by the presence of hydrophilic and hydrophobic groups that allow it to effectively encapsulate hydrophobic and hydrophilic drugs.[45] The presence of additional hydroxyl (OH) groups from cholesterol could be responsible for the broad absorption band at 3330 cm^{-1}. The distinct peaks at 2931 cm^{-1}, 2895 cm^{-1}, and 1464 cm^{-1} could be attributed to asymmetric stretching vibrations of the CH$_2$ and CH$_3$ groups of niosomes.[46] The sharp peaks at 1168 cm^{-1} and 1047 cm^{-1} correspond to ring deformation in CH$_2$ bending and in-plane C–H bending, respectively. The bands between 900 and 675 cm^{-1} represent the CH out-of-plane bending, and

the band at 840 cm^{-1} indicates C–C–C stretching. FTIR spectra of doxorubicin, vitexin, and both drugs loaded niosomes (Fig. 2B) exhibited all the characteristic peaks of the niosomes, suggesting that no chemical reaction occurred between the drugs and niosomes. When gold nanoparticles were added to NIODV (Fig. 2C and D), the stretching frequency of C=O of the citrate ligands shifted from 1635 cm^{-1} to 1651 cm^{-1}, indicating an interaction between the carbonyl group and the hydrophilic surface of the niosomes. Conjugation of cetuximab showed its characteristic peak at 1637 cm^{-1}, suggesting a π back bond between the gold nanoparticle and the cetuximab antibody resulting in the formation of a covalent bond between the two entities.[47,48] The blue shift observed in the carbonyl stretching of gold nanoparticle conjugated

NIODV compared to NIODVC confirmed the conjugation of cetuximab with the gold nanoparticles.

3.2. High resolution electron microscopic analysis of virgin and drug loaded niosomes

Size and surface morphology of all niosome formulations were evaluated by scanning electron microscopy (SEM) (Fig. 3) and DLS measurements respectively. The niosomes were stained with phospho-tungstic acid (1%) at room temperature and visualized under a high resolution scanning electron microscope. Niosomes were spherical, with a smooth outer surface, and contained a large internal aqueous area. The outer lipophilic domain appeared dark, while the inner hydrophilic domain was light. The average size of virgin niosomes was 513 nm (Fig. 3A), whereas niosomes with both doxorubicin and vitexin had a larger lipophilic domain, resulting in an average size of almost 614 nm (Fig. 3D).

A high resolution transmission electron microscope (HRTEM) was used to characterize the antibody conjugated niosomes (Fig. 4). The Turkevich method used in the present study is a popular way to synthesize spherical gold nanoparticles because the citrate ions used are biocompatible with good crosslinking ability.[26] Citrate acts as a stabilizer for the gold nanoparticles during the reaction and it also alters the pH of the system to around 6.7, which influences the size of gold nanoparticles, resulting in nearly monodisperse gold nanoparticles (20 to 40 nm). The absorption peak for gold nanoparticles was at 520 nm (Fig. 4A)[49] but the maximum absorption of gold nanoparticles in NIODVC was at 557 nm. This shift could be attributed to the changes in the local refractive index because of protein adhesion.[50] Gold nanoparticles were spherical (Fig. 4B), and the average particle size was around 17 nm (Fig. 4C). The niosomes had uniform,

smooth bilayer morphology, and the size distribution was within the range of 0.34 to 0.4 μm. TEM images showed that the gold nanoparticles were found attached to the hydrophilic layer of the niosome (Fig. 4D and E) and the EDX analysis confirmed the same (Fig. 4F). EDX analysis confirmed the presence of carbon (K: 0.27 keV) and gold emission lines (M: 2.23 keV). Carbon and oxygen accounted for 88.2, and 5.86 wt% which could be attributed to both niosomes and antibody, while Au atoms on the surface of niosomes accounted for the remaining 5.86 wt%.

3.3. *In vitro* drug release kinetics

The release of doxorubicin, vitexin, and dual drugs from niosomes was studied in PBS (pH 7.4) at 37 °C. The amount of drug released was determined at regular time intervals for a period of 96 h and the cumulative release (mean ± standard deviation) against time was plotted (Fig. 5). A biphasic drug release pattern was found, with an initial burst release for 3–9 hours followed by a controlled release for 72 h. The burst release could be attributed to the release of the drug from the surface of the niosomes and smaller niosomes,[51] while the controlled release could be attributed to drug diffusion through the vesicle bilayer. The highest percentage of drug was released from NIODV (85% for D and 63% for V), followed by NIOD (69%) and NIOV (49%). The differences in the release of same drugs in two different formulations could be attributed to the differences in size. The size of dual drug loaded niosomes was ∼614 nm. In general, the presence of high levels of cholesterol in niosome formulations enhances membrane stability and increases the hydrophobicity of the vesicles. As a result, drug release from the niosomes is slowed due to reduced permeability across the bilayer membrane.[52] Previous studies have reported that niosomes loaded with timolol maleate for glaucoma treatment exhibited a sustained release pattern, and the entire drug was released from the vesicles in approximately 24 h but the free form of the drug was released completely within 4 h.[53] Similarly, doxycycline, an ocular antibiotic, was fully released within the initial hour in its free form, while its niosome formulation sustained the release up to 20 h.[54] In NIODVC the release of doxorubicin and vitexin was sustained up to 96 h.

The correlation coefficient (R^2) of various mathematical models used to fit the drug release profiles is tabulated in Table 3. Drug release from the niosomes followed different kinetics depending on the formulation. NIOD fits the Korsmeyer–Peppas model, suggesting a non-Fickian diffusion and erosion mechanism (Fig. S1, ESI†), whereas NIOV followed zero order kinetics with an initial burst release followed by continuous release (Fig. S2, ESI†). In the case of NIODV, both doxorubicin and vitexin followed Higuchi kinetics, indicating a diffusion-based drug release from the vesicles (Fig. S3, ESI†). These results were in line with meta-analysis findings of different release kinetics extrapolated from different drug delivery vehicles.[55]

3.4. Screening of niosomes efficiency against breast cancer cells *in vitro*

The cytotoxicity of virgin niosomes, drug loaded niosomes, and gold nanoparticles at a fixed concentration (10 μM) was tested
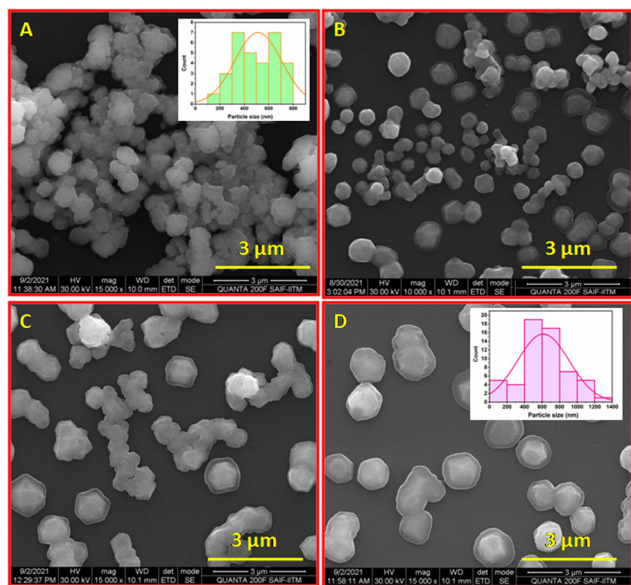

Fig. 3 High resolution scanning electron microscopic images of niosomes (A) (inset: particle size distribution), NIOD (B), NIOV (C), and NIODV (D) (inset: particle size distribution).
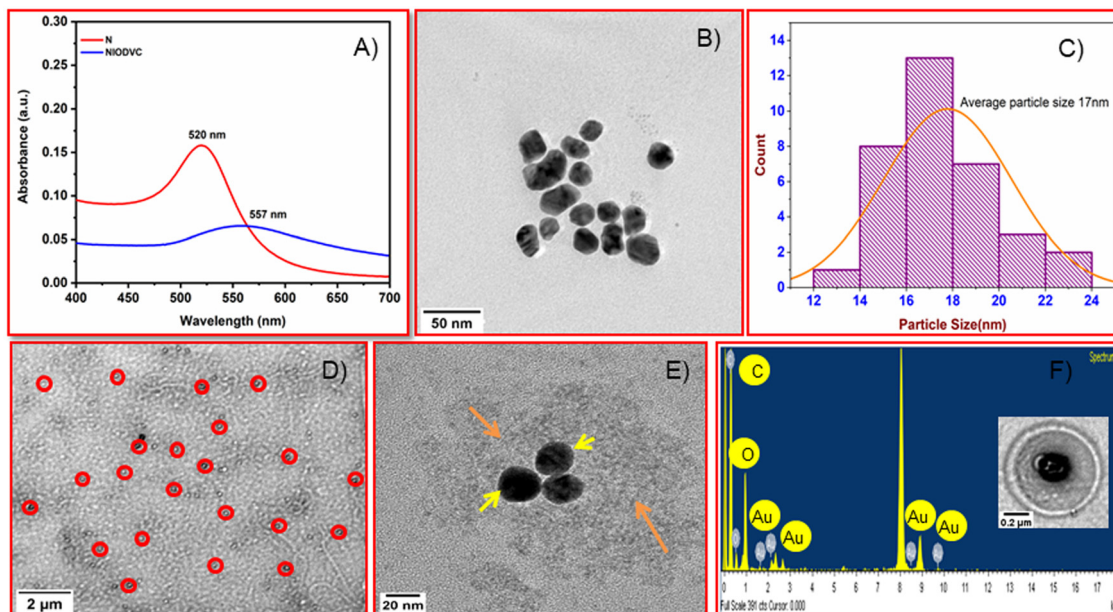
Fig. 4 Characterization of nanoparticles and niosomes: UV-visible spectrum (A), transmission electron microscopic images (B) and particle size distribution of gold nanoparticles (C). Low (D) and high (E) magnification transmission electron microscopic images and energy-dispersive X-ray spectroscopy of NIODVC.
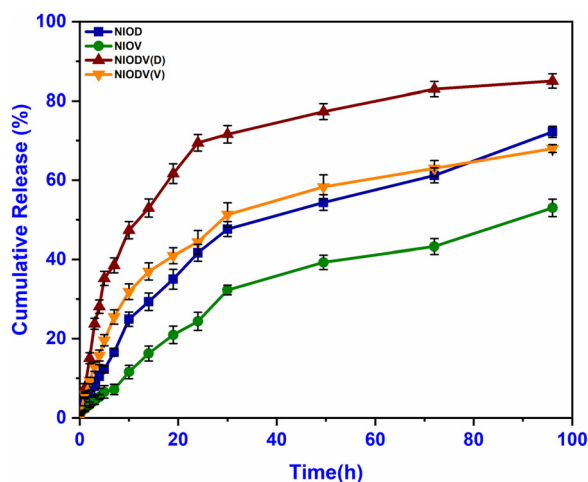

Fig. 5 *In vitro* drug release profiles of niosome formulations containing doxorubicin (NIOD), vitexin (NIOV), and both drugs (NIODV).

against MDA-MB-231 cells (Fig. 6). MTT assay showed that virgin niosomes and gold nanoparticles had minimal cytotoxicity, while NIODVC was more cytotoxic (35% cell viability) than NIODV (45% cell viability). The delivery of doxorubicin and

vitexin together was 1.5 times higher than individual drug delivery, revealing the synergistic effects. Combination of flavonoids and anticancer drugs helps to overcome the systemic toxicity of chemotherapeutic agents and increases the anticancer effect of the drug at lower concentrations.[56] Similar results have also been reported with the co-delivery of doxorubicin and quercetin from PEGylated niosomes.[57]

Fluorescence of doxorubicin was used to detect the cellular uptake in MDA-MB-231 cells; cells were counter stained with DAPI after niosome treatment to visualize the nucleus (Fig. 7). Cetuximab conjugated niosomes exhibited strong fluorescence intensity in the cytoplasm compared to the NIODV which could be attributed to the specificity and selective binding of the antibody to the epidermal growth factor receptor. This opens a new window for targeted cancer treatment.

The FDA/PI staining showed niosome induced apoptosis in MDA-MB-231 cells (Fig. S4, ESI†). FDA penetrates the live cells and emits green fluorescence, while PI stains the dead cell nuclei red. Cells treated with NIOD, NIOV, and NIODV displayed characteristics of early and late apoptotic cells. Doxorubicin induces apoptosis by inhibiting DNA replication and repair,[58] while vitexin promotes apoptosis by inducing oxidative stress and inhibiting cell proliferation.[59] The increased apoptosis

Table 3 Release kinetics of niosome formulations

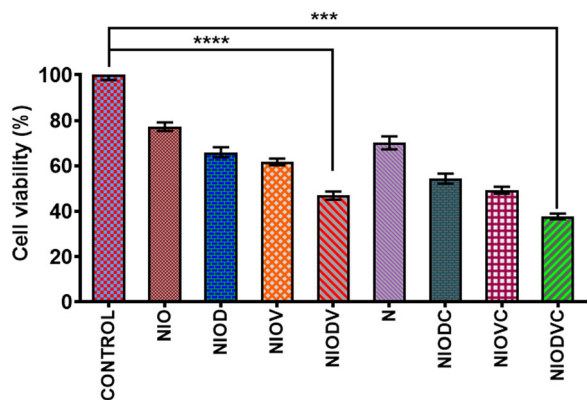| Formulation code	Correlation coefficient (R^2)				
	Zero order	First order	Higuchi	Hixson–Crowell	Korsmeyer–Peppas
NIOD	0.973	0.985	0.986	0.979	0.988
NIOV	0.993	0.992	0.951	0.946	0.976
NIODV (DOX release)	0.885	0.414	0.976	0.944	0.742
NIODV (VIT release)	0.925	0.786	0.988	0.952	0.989

Fig. 6 Cytotoxicity of virgin and drug loaded niosomes against MDA-MB-231 cells after 24 hours of incubation. Results are presented as the mean ± standard deviation (SD) of three independent experiments. ***$p < 0.001$, ****$p < 0.0001$.

with the combined delivery of doxorubicin and vitexin could be attributed to the synergistic effect of the combination of these drugs.

3.5. *In vivo* efficiency of niosomes on a mouse tumor model: systemic *vs.* local delivery

The *in vivo* efficacy of dual drug loaded niosomes, with and without antibody conjugation, was assessed on a 4T1 cell induced tumor model in BALB/c mice using two distinct delivery methods. For localized delivery, the niosomes were injected at the fourth mammary tumor tissue and to determine

their efficiency in targeted delivery, the niosomes were injected intravenously through the caudal vein. Representative images of the dissected tumor after 20 days of treatment are represented in Fig. 8 showing the changes in tumor volume, tumor weight and body weight. The average tumor volume was 796.7 ± 285.3 mm^3 in the tumor group (Group 2). In the case of NIODV when delivered locally it was 313 ± 56 mm^3 (Group-3), and for systemic delivery it was 181.7 ± 41 mm^3 (Group-4). In the case of NIODVC, when delivered locally it was 126.8 ± 50.7 mm^3 (Group-5), and for intravenous it was 240 ± 43.8 mm^3 (Group-6). All the niosome formulations exhibited significant anti-tumor activity compared to the tumor group. Tumor shrinkage was higher with NIODV when delivered systemically (2.54 fold increase than local injection). Interestingly, the tumor shrinkage was higher with NIODVC when delivered locally compared to systemic delivery (6.28 and 4.38 fold increase), which could be attributed to the efficiency of specific binding of cetuximab to the epidermal growth factor receptor (EGFR), which is overexpressed in many cancer cells.[60] The difference in systemic delivery could be attributed to the bioavailability of NIODVC. Similar results were observed with liposomes conjugated with Fab fragments of cetuximab, which resulted in a 6 fold increase in drug accumulation in MDA-MB-468 human breast cancer xenografts.[61]

Fig. 9 shows quantitative mRNA expression profiles of cell proliferative genes such as BRCA1, cMYC, EpCAM, iCAM and MMP9 and inflammatory genes iNOX and NF-κB in mammary tissue. In the tumor group, there was an increase in the expression levels of genes related to proliferation and inflammation.
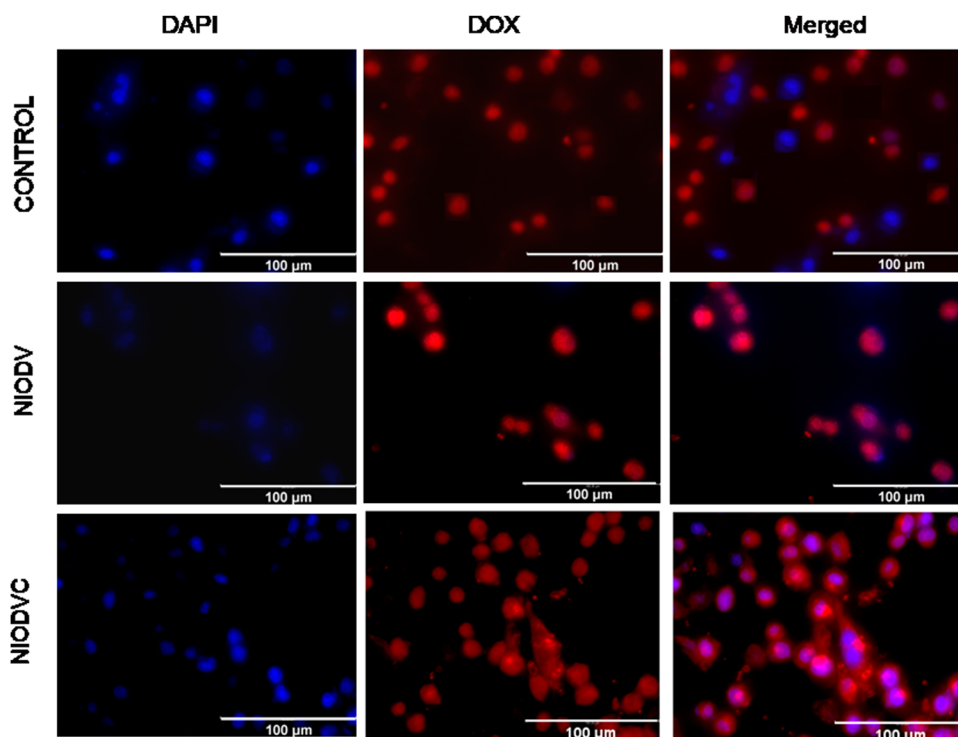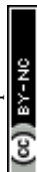

Fig. 7 MDA-MB-231 cellular uptake of niosome formulations counter stained with DAPI (blue) and doxorubicin (red). The merged image shows the co-localization of both DAPI and doxorubicin inside the cells.
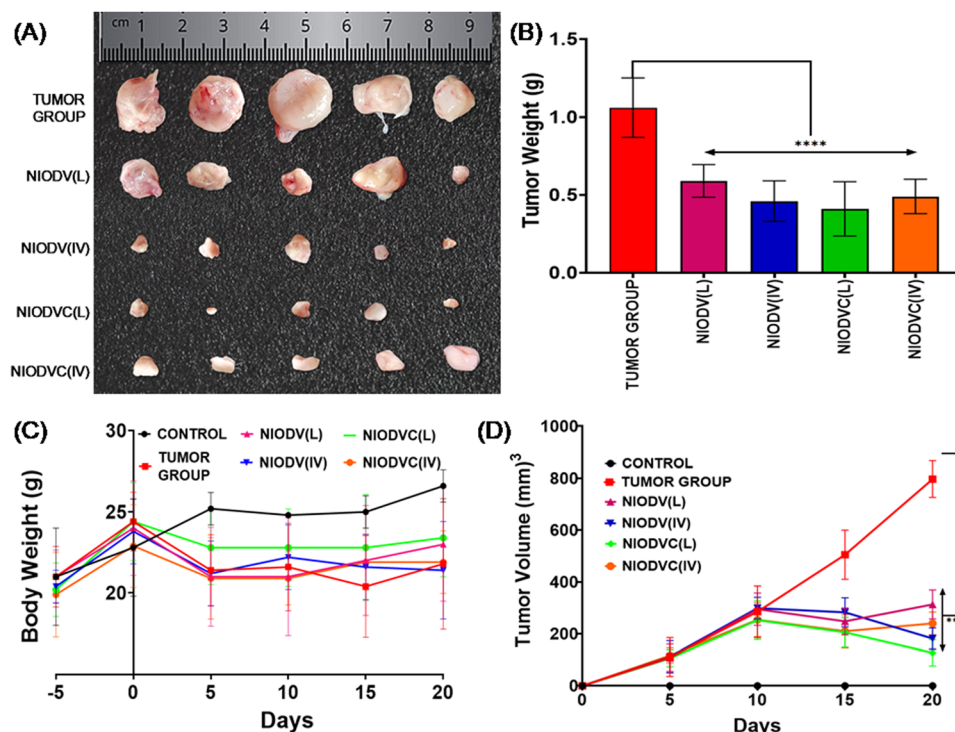
Fig. 8 Photographic images captured 20 days after niosome treatment, illustrate changes in the average tumor volume (A) and tumor weight (B), body weight (C) and tumor volume (D). Note: ***$p < 0.001$, indicating statistical significance.
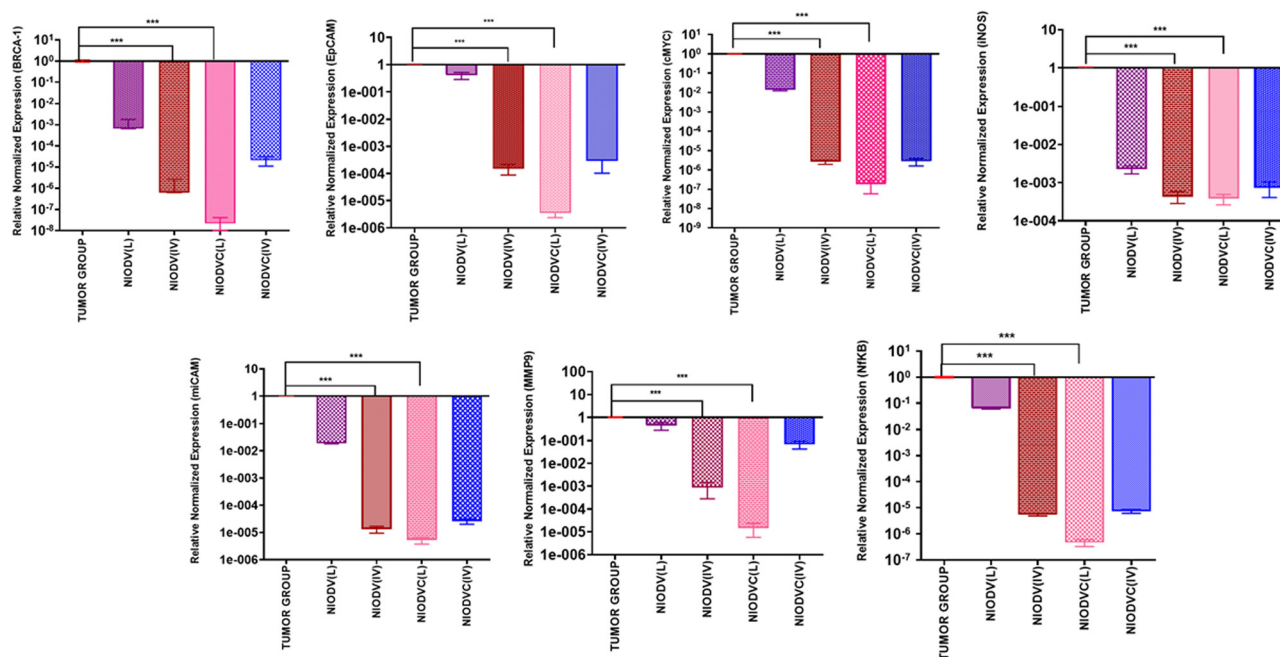

Fig. 9 Gene expression levels of BRCA1, EpCAM, cMYC, iNOS, miCAM, MMP9, and NFKB in 4T1 tumor cells after treatment with niosomes. The expression levels were normalized to the reference gene beta actin and presented as fold change relative to the control group. ***$P < 0.01$.

However, the expression levels of these genes were significantly altered in the niosome treated mice. Previous reports have shown that cetuximab combined with chemotherapeutic drugs was effective in treating TNBC.[62,63] Cetuximab binds to the epidermal growth factor receptor (EGFR), which is important in metastasis, tumorigenesis, drug resistance, and cell proliferation.[62,63]

Doxorubicin acts as a DNA inter-chelator and inhibits the topoisomerase II enzyme resulting in the inhibition of cancer cell growth; it also causes dsDNA damage and activates downstream apoptotic pathways.[64] Similarly, vitexin promotes apoptosis and cell cycle arrest.[65]

In the present study, elevated expression of BRCA1, cMYC, EpCAM, iCAM, MMP9, iNOS, and NFκB in the mammary tissues of the tumor group was observed. In contrast, mRNA expression of tumour suppressor gene BRCA1 was downregulated in the case of niosome treated groups. However, the local delivery of NIODVC resulted in decreased expression of proliferative, angiogenic, and inflammatory genes. It exerts inhibitory effects on cell migration and angiogenesis by down-regulating cMYC, EpCAM, iCAM, and MMP9.[66] Additionally, the down-regulation of NF-κB and iNOS indicates reduced inflammation and immune responses.[67]

Breast cancer susceptibility gene 1 (BRCA1) primarily a tumor suppressor gene plays a crucial role in DNA repair, replication fork protection, cell cycle regulation, and preservation of genome stability.[68] Mutations or abnormalities in the BRCA1 gene make the cell more vulnerable to various cancers. Cellular myelocytomatosis (c-MYC) is a proto-oncogene that encodes a multifunctional transcription factor. It plays an important role in cell cycle progression from G1 to S phase and is overexpressed in various cancers, including breast cancer.[69] The epithelial cell adhesion molecule (EpCAM) is a transmembrane glycoprotein that is overexpressed in many epithelial cancers and it is involved in gene regulation, cell proliferation, cancer stemness, and interactions with cell adhesion molecules.[70] The intracellular adhesion molecule (iCAM) is a transmembrane glycoprotein receptor that plays a vital role in cell adhesion, cell signaling, and transendothelial migration. Overexpression of iCAM has been reported in various malignancies, including TNBC.[71] Matrix metalloprotease (MMP)-9 is a zinc- and calcium-dependent protease that digests and remodels a wide range of extracellular matrix components. It is overexpressed in various cancer cells during invasion and plays a key role in tumorigenesis by inducing angiogenesis in the tumor microenvironment.[72] Nuclear factor kappa B subunit 1 (NFκB) is a transcription factor that regulates the activation of various proinflammatory cytokine genes.[73] Inducible nitric oxide synthase (iNOS) is a pro-inflammatory enzyme that is involved in various chronic inflammatory conditions, including breast cancer.[74]

Fig. 10(A)–(F) shows the histopathological analysis of mammary tissue of control and experimental groups. The group I control animal showed normal histotype of ductal and stromal elements and normal mammary fat tissue (Fig. 10A). In contrast, the tumor group (Group II) showed severely infiltrated neoplastic ductal epitheloid cells with pleomorphic and hyperchromatic nuclei, and the average mitotic index was 5.4 per 10 high power field (HPF, 400×) (Fig. 10B). The niosome treated mice (Groups III to VI) exhibited residual tumours with usual ductal hyperplasia, which is a common mild-cancerous to noncancerous breast condition characterized by an overgrowth of cells in the ducts of the breast. In the case of NIODV delivered locally (Group III) there were mild infiltrating hyperplastic mammary epitheloid cells with moderate fibrosis, and
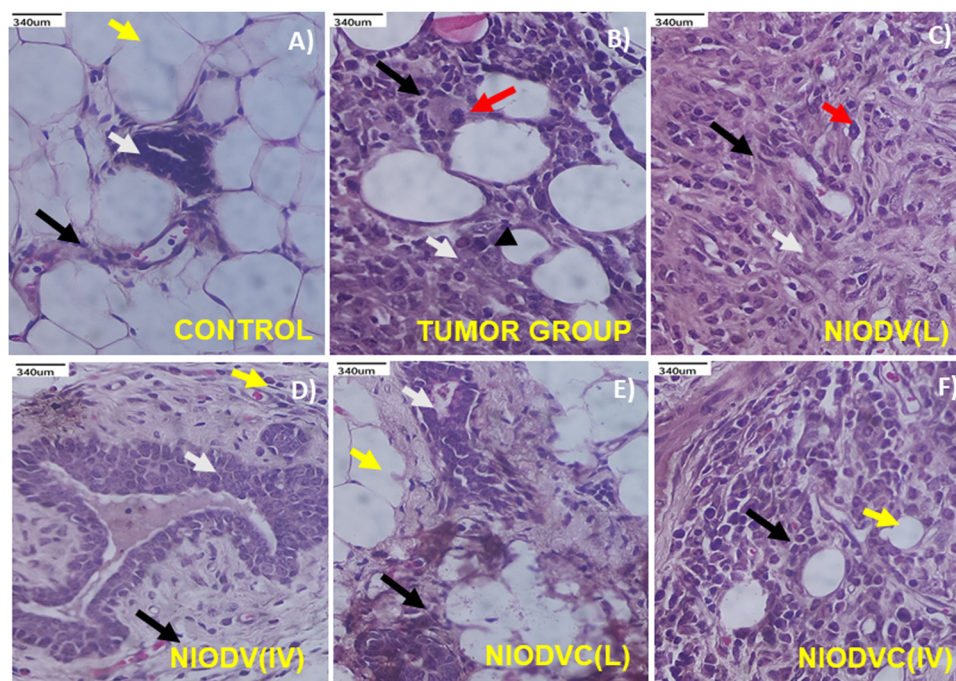

Fig. 10 Histopathological analysis of control (A) and tumor group (B) with infiltrating ductal adenocarcinoma of the breast – grade II. NIODV injected locally (C) and systemically (D) with residual infiltrating ductal adenocarcinoma of the breast – grade II and ductal hyperplasia and inflammatory infiltration. NIODVC injected locally (E) and systemically (F) with ductal epithelioid hyperplasia and inflammatory infiltration. Black arrow – mononuclear inflammatory infiltrates, white arrow – ductal elements, yellow arrow – fat component of breast tissue, red arrow – tumor giant cells.
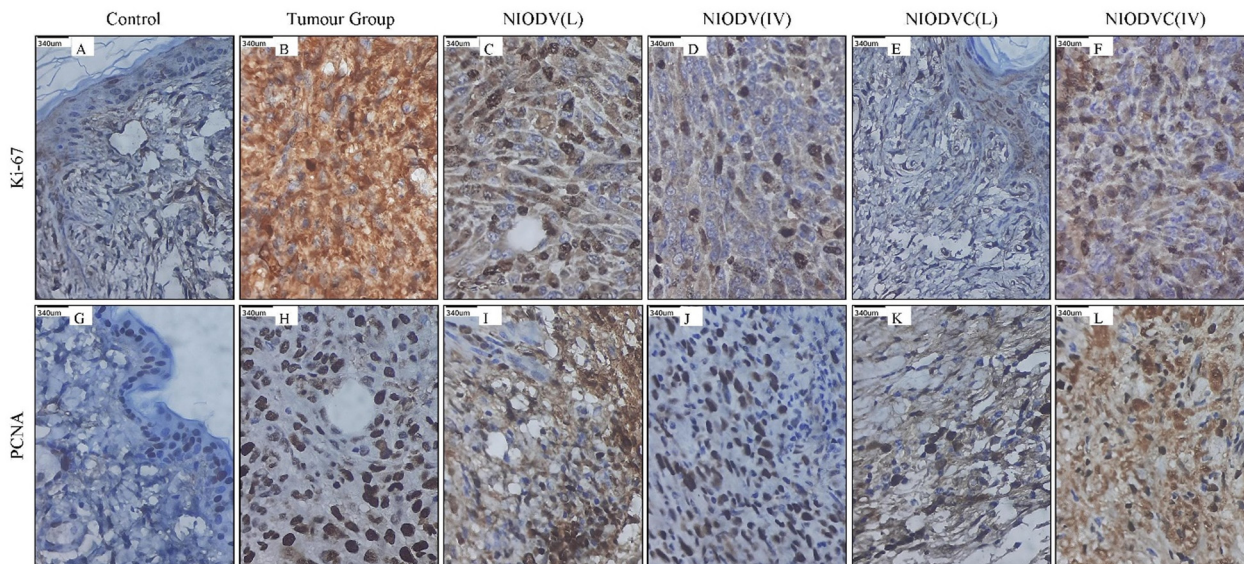
Fig. 11 Representative images of immunohistochemical staining for Ki-67 in control (A), tumor group (B), NIODV injected locally (C) and systemically (D), and NIODVC injected locally (E) and systemically (F) and for PCNA in control (G), tumor group (H), NIODV injected locally (I) and systemically (J), and NIODVC injected locally (K) and systemically (L). Brown staining indicates a positive expression of Ki-67 or PCNA.

the mitotic index reduced to 2.7 per 10 HPF (Fig. 10C); when it was delivered systemically (Group IV) there was usual ductal hyperplasia with mild fibrosis; and no mitotic figures were observed (Fig. 10D) in the case of NIODVC delivered locally (Group V). The tissue showed a normal architecture with mild fibrosis, and no mitotic figures (Fig. 10E) whereas when it was delivered systemically (Group VI) the tissues showed infiltrated hyperplastic mammary cell carcinoma with fibrosis, and an average mitotic index of 2.2 per 10 HPF (Fig. 10F). Histopathological analysis of the tumour group showed invasive ductal carcinoma (grade 2 to 3) with increased mitotic activity, whereas locally delivered NIODVC showed regression in tumour lesion with improved ductal architecture and reduced mitotic index.

Fig. 11 shows the immunohistochemical staining of Ki67 and PCNA in control, tumor, and niosome treated groups respectively. There was a significant increase in the level of Ki67 and PCNA in the tumor group (Group-2), indicating active tumor cell proliferation. However, the level of these markers decreased significantly in niosome treated groups. In the present study, the local delivery of NIODVC (Group-5) resulted in the complete absence of Ki67 and PCNA expression in the ductal epithelial cells, which is in line with the tumor shrinkage volume, followed by NIODV (Group-4), NIODVC (Group-6), and NIODV (Group-3). Ki-67 is a 358 kDa nonhistone nuclear protein, which is overexpressed in actively dividing cells and it is widely used as a marker to assess the proliferative index in various cancers, including breast cancer.[75] Proliferating cell nuclear antigen (PCNA) is a 36 kDa nonhistone nuclear cyclin protein, which is predominantly expressed in cells that undergo cell division and it is also used as a proliferative marker in several cancers.[76] The present study revealed that conjugation of cetuximab helps to achieve the anti-proliferative effect of the treatment, as evidenced by the complete absence of Ki67 and PCNA expression in the ductal epithelial cells after local administration.

4. Conclusion

In conclusion, the current study demonstrated the successful formulation of niosomes with high encapsulation efficiency (doxorubicin: 85% and vitexin: 67%) and stability. Cetuximab conjugated doxorubicin and vitexin loaded niosomes showed promising anti-tumor activity in 4T1 induced breast cancer mouse models. The release profile of doxorubicin, vitexin and the combination of both drugs exhibited a biphasic pattern, with an initial burst release followed by sustained slow release. The combined delivery of doxorubicin and vitexin from NIODV enhanced cellular uptake and cytotoxicity. NIODVC exhibited higher anti-tumor activity than other niosome formulations which are not conjugated with the antibody. Histopathological analysis revealed the potential anti-inflammatory effects of the niosome formulation on breast tissue, with downregulation of all genes tested.

Conflicts of interest

None.

Acknowledgements

References

1 L. Wilkinson and T. Gathani, *Br. J. Radiol.*, 2022, **95**, 20211033.

2 L. Minig, M. G. Patrono, N. Romero, J. F. Rodriguez Moreno and J. Garcia-Donas, *World J. Clin. Oncol.*, 2014, **5**, 86–92.

3 S. Licata, A. Saponiero, A. Mordente and G. Minotti, *Chem. Res. Toxicol.*, 2000, **13**, 414–420.

4 P. S. Rawat, A. Jaiswal, A. Khurana, J. S. Bhatti and U. Navik, *Biomed. Pharmacother.*, 2021, **139**, 111708.

5 G. Du, H. Lin, M. Wang, S. Zhang, X. Wu, L. Lu, L. Ji and L. Yu, *Cancer Chemother. Pharmacol.*, 2010, **65**, 277–287.

6 M. Hamzeh-Mivehroud, S. Rahmani, M.-A. H. Feizi, S. Dastmalchi and M.-R. Rashidi, *Arch. Pharm.*, 2014, **347**, 738–747.

7 G. Scambia, F. O. Ranelletti, P. B. Panici, R. De Vincenzo, G. Bonanno, G. Ferrandina, M. Piantelli, S. Bussa, C. Rumi, M. Cianfriglia and S. Mancuso, *Cancer Chemother. Pharmacol.*, 1994, **34**, 459–464.

8 R. Václavíková, E. Kondrová, M. Ehrlichová, A. Boumendjel, J. Kovář, P. Stopka, P. Souček and I. Gut, *Bioorg. Med. Chem.*, 2008, **16**, 2034–2042.

9 F. Babaei, A. Moafizad, Z. Darvishvand, M. Mirzababaei, H. Hosseinzadeh and M. Nassiri-Asl, *Food Sci. Nutr.*, 2020, **8**, 2569–2580.

10 X. Che, X. Wang, J. Zhang, C. Peng, Y. Zhen, X. Shao, G. Zhang and L. Dong, *Am. J. Transl. Res.*, 2016, **8**, 3319–3328.

11 R. Bartelds, M. H. Nematollahi, T. Pols, M. C. A. Stuart, A. Pardakhty, G. Asadikaram and B. Poolman, *PLoS One*, 2018, **13**, e0194179.

12 A. Sankhyan and P. Pawar, *J. Appl. Pharm. Sci.*, 2012, **2**(6), 20–32.

13 D. Pando, M. Matos, G. Gutiérrez and C. Pazos, *Colloids Surf., B*, 2015, **128**, 398–404.

14 C. A. Hunter, T. F. Dolan, G. H. Coombs and A. J. Baillie, *J. Pharm. Pharmacol.*, 1988, **40**, 161–165.

15 N. G. Kotla, B. Chandrasekar, P. Rooney, G. Sivaraman, A. Larrañaga, K. V. Krishna, A. Pandit and Y. Rochev, *ACS Biomater. Sci. Eng.*, 2017, **3**, 1262–1272.

16 R. Muzzalupo, L. Pérez, A. Pinazo and L. Tavano, *Int. J. Pharm.*, 2017, **529**, 245–252.

17 S. Khambata-Ford, C. T. Harbison, L. L. Hart, M. Awad, L.-A. Xu, C. E. Horak, S. Dakhil, R. C. Hermann, T. J. Lynch and M. R. Weber, *J. Clin. Oncol.*, 2010, **28**, 918–927.

18 J. A. Khan, R. A. Kudgus, A. Szabolcs, S. Dutta, E. Wang, S. Cao, G. L. Curran, V. Shah, S. Curley, D. Mukhopadhyay, J. D. Robertson, R. Bhattacharya and P. Mukherjee, *PLoS One*, 2011, **6**, e20347.

19 S.-H. Ryu, S.-w Lee, Y.-J. Yang, S. Y. Song, J. H. Kim, E. K. Choi and S. D. Ahn, *Lung Cancer*, 2012, **77**, 482–487.

20 M. Z. Ahmad, S. Akhter, Z. Rahman, S. Akhter, M. Anwar, N. Mallik and F. J. Ahmad, *J. Pharm. Pharmacol.*, 2013, **65**, 634–651.

21 W. H. De Jong and P. J. Borm, *Int. J. Nanomed.*, 2008, **3**, 133–149.

22 M. M. Joseph, S. R. Aravind, S. Varghese, S. Mini and T. T. Sreelekha, *Colloids Surf., B*, 2013, **104**, 32–39.

23 J. Sakamoto, A. Annapragada, P. Decuzzi and M. Ferrari, *Expert Opin. Drug Delivery*, 2007, **4**, 359–369.

24 H. Xie, S. Gu, J. Zhang, Q. Hu, X. Yu and J. Kong, *C. R. Chim*, 2018, **21**, 104–111.

25 I. F. Uchegbu and S. P. Vyas, *Int. J. Pharm.*, 1998, **172**, 33–70.

26 J. Turkevich, P. C. Stevenson and J. Hillier, *Discuss. Faraday Soc.*, 1951, **11**, 55–75.

27 Y. Qian, M. Qiu, Q. Wu, Y. Tian, Y. Zhang, N. Gu, S. Li, L. Xu and R. Yin, *Sci. Rep.*, 2014, **4**, 7490.

28 B. Sivakumar, R. G. Aswathy, Y. Nagaoka, S. Iwai, K. Venugopal, K. Kato, Y. Yoshida, T. Maekawa and D. N. Sakthi Kumar, *RSC Adv.*, 2013, **3**, 20579–20598.

29 B. Kocatürk and H. H. Versteeg, *J. Vis. Exp.*, 2015, **8**, 51967.

30 A. Manigandan, V. Handi, N. S. Sundaramoorthy, R. Dhandapani, J. Radhakrishnan, S. Sethuraman and A. Subramanian, *Bioconjugate Chem.*, 2018, **29**, 275–286.

31 A. Rodallec, C. Vaghi, J. Ciccolini, R. Fanciullino and S. Benzekry, *PLoS One*, 2022, **17**, e0274886.

32 A. A. Samadani, N. Nikbakhsh, S. Fattahi, R. Pourbagher, S. M. Aghajanpour Mir, N. Mousavi Kani, Z. Abedian and H. Akhavan-Niaki, *Int. J. Mol. Cell. Med.*, 2015, **4**, 54–59.

33 N. Nordin, S. K. Yeap, H. S. Rahman, N. R. Zamberi, N. E. Mohamad, N. Abu, M. J. Masarudin, R. Abdullah and N. B. Alitheen, *Molecules*, 2020, **25**, 2670.

34 J. D. Bancroft and C. Layton, in *Bancroft's Theory and Practice of Histological Techniques*, ed. S. K. Suvarna, C. Layton and J. D. Bancroft, Elsevier, 8th edn, 2019, pp. 1–557.

35 E. A. Essa, *Asian J. Pharm.*, 2010, **4**(4), 227–233.

36 W. B. Liechty and N. A. Peppas, *Eur. J. Pharm. Biopharm.*, 2012, **80**, 241–246.

37 M. Chen, X. Liu and A. Fahr, *Int. J. Pharm.*, 2011, **408**, 223–234.

38 C. Detroja, S. Chavhan and K. Sawant, *Sci. Pharm.*, 2011, **79**, 635–651.

39 M. Ghazwani, U. Hani, A. Alam and M. H. Alqarni, *Gels*, 2023, **9**, 401.

40 F. Rezaie Amale, S. Ferdowsian, S. Hajrasouliha, R. Kazempoor, A. Mirzaie, M. Sedigh Dakkali, I. Akbarzadeh, S. Mohammadmahdi Meybodi and M. Mirghafouri, *Adv. Powder Technol.*, 2021, **32**, 4711–4722.

41 S. Krasnici, A. Werner, M. E. Eichhorn, M. Schmitt-Sody, S. A. Pahernik, B. Sauer, B. Schulze, M. Teifel, U. Michaelis, K. Naujoks and M. Dellian, *Int. J. Cancer*, 2003, **105**, 561–567.

42 Y. Li and A. K. Mitra, *Pharm. Res.*, 1996, **13**, 76–79.

43 K. Banerjee, S. Banerjee, S. Das and M. Mandal, *J. Colloid Interface Sci.*, 2015, **453**, 48–59.

44 B. Nasseri, *Int. J. Pharm.*, 2005, **300**, 95–101.

45 V. Sharma, S. Anandhakumar and M. Sasidharan, *Mater. Sci. Eng., C*, 2015, **56**, 393–400.

46 W. Ren, G. Tian, S. Jian, Z. Gu, L. Zhou, L. Yan, S. Jin, W. Yin and Y. Zhao, *RSC Adv.*, 2012, **2**, 7037–7041.

47 L. García-Fernández, J. Garcia-Pardo, O. Tort, I. Prior, M. Brust, E. Casals, J. Lorenzo and V. F. Puntes, *Nanoscale*, 2017, **9**, 6111–6121.

48 W. Haiss, N. T. K. Thanh, J. Aveyard and D. G. Fernig, *Anal. Chem.*, 2007, **79**, 4215–4221.

49 K. Tripathi and J. D. Driskell, *ACS Omega*, 2018, **3**, 8253–8259.

50 X. Liu, M. Atwater, J. Wang and Q. Huo, *Colloids Surf., B*, 2007, **58**, 3–7.

51 L. Thomas and V. Viswanad, *Sci. Pharm.*, 2012, **80**, 731–748.

52 A. A. Ramadan, S. A. Eladawy, A. S. M. A. El-Enin and Z. M. Hussein, *J. Pharm. Invest.*, 2020, **50**, 59–70.

53 V. Gugleva, S. Titeva, S. Rangelov and D. Momekova, *Int. J. Pharm.*, 2019, **567**, 118431.

54 C. Mircioiu, V. Voicu, V. Anuta, A. Tudose, C. Celia, D. Paolino, M. Fresta, R. Sandulovici and I. Mircioiu, *Pharmaceutics*, 2019, **11**, 140.

55 M. Siddiqui, B. Abdellatif, K. Zhai, A. Liskova, P. Kubatka and D. Büsselberg, *Cancers*, 2021, **13**, 1576.

56 M. Hemati, F. Haghiralsadat, F. Yazdian, F. Jafari, A. Moradi and Z. Malekpour-Dehkordi, *Artif. Cells, Nanomed., Biotechnol.*, 2019, **47**, 1295–1311.

57 M. Giorgio, M. Pierantonio, S. Emanuela, C. Gaetano and G. Luca, *Pharmacol. Rev.*, 2004, **56**, 185.

58 Y. Zhou, Y. E. Liu, J. Cao, G. Zeng, C. Shen, Y. Li, M. Zhou, Y. Chen, W. Pu, L. Potters and Y. E. Shi, *Clin. Cancer Res.*, 2009, **15**, 5161–5169.

59 M. Frattini, P. Saletti, F. Molinari and S. De Dosso, *Gastrointest. Cancer: Targets Ther.*, 2015, 21–38.

60 C. Mamot, D. C. Drummond, C. O. Noble, V. Kallab, Z. Guo, K. Hong, D. B. Kirpotin and J. W. Park, *Cancer Res.*, 2005, **65**, 11631–11638.

61 T. Tanei, D. S. Choi, A. A. Rodriguez, D. H. Liang, L. Dobrolecki, M. Ghosh, M. D. Landis and J. C. Chang, *Breast Cancer Res.*, 2016, **18**, 6.

62 N. E. Mohamad, N. Abu, S. K. Yeap, K. L. Lim, M. F. Romli, S. A. Sharifuddin, K. Long and N. B. Alitheen, *Nutr. Metab.*, 2019, **16**, 49.

63 H. A. Wahba and H. A. El-Hadaad, *Cancer Biol. Med.*, 2015, **12**, 106–116.

64 A. Kumar, J. White, R. James Christie, N. Dimasi and C. Gao, in *Annual Reports in Medicinal Chemistry*, ed. R. A. Goodnow, Academic Press, 2017, vol. 50, pp. 441–480.

65 Y. Chen, X. Yuan, C. Pei, Z. Deng, X. Du, J. Liang, L. He and S. Hou, *J. Funct. Foods*, 2022, **95**, 105190.

66 S. H. Tsai, S. Y. Lin-Shiau and J. K. Lin, *Br. J. Pharmacol.*, 1999, **126**, 673–680.

67 M. Feng, C. Feng, Z. Yu, Q. Fu, Z. Ma, F. Wang, F. Wang and L. Yu, *Int. J. Clin. Exp. Med.*, 2015, **8**, 346–357.

68 X. Fu, W. Tan, Q. Song, H. Pei and J. Li, *Front. Cell Dev. Biol.*, 2022, **10**, 813457.

69 M. E. Menezes, S. K. Das, L. Emdad, J. J. Windle, X. Y. Wang, D. Sarkar and P. B. Fisher, *Adv. Cancer Res.*, 2014, **121**, 331–382.

70 S. Z. Eslami, L. E. Cortés-Hernández and C. Alix-Panabières, *Cells*, 2020, **9**, 1836.

71 H. Wei, Z. Wang, Y. Kuang, Z. Wu, S. Zhao, Z. Zhang, H. Li, M. Zheng, N. Zhang, C. Long, W. Guo, C. Nie, H. Yang and A. Tong, *Front. Immunol.*, 2020, **11**, 573823.

72 H. Huang, *Sensors*, 2018, **18**, 3249.

73 T. Liu, L. Zhang, D. Joo and S.-C. Sun, *Signal Transduction Targeted Ther.*, 2017, **2**, 17023.

74 M. A. Cinelli, H. T. Do, G. P. Miley and R. B. Silverman, *Med. Res. Rev.*, 2020, **40**, 158–189.

75 A. Sahin and H. Zhang, in *Pathobiology of Human Disease*, ed. L. M. McManus and R. N. Mitchell, Academic Press, San Diego, 2014, pp. 934–951, DOI: 10.1016/B978-0-12-386456-7.03204-4.

76 L. H. Malkas, B. S. Herbert, W. Abdel-Aziz, L. E. Dobrolecki, Y. Liu, B. Agarwal, D. Hoelz, S. Badve, L. Schnaper, R. J. Arnold, Y. Mechref, M. V. Novotny, P. Loehrer, R. J. Goulet and R. J. Hickey, *Proc. Natl. Acad. Sci. U. S. A.*, 2006, **103**, 19472–19477.